UNIVERSITY OF BIRMINGHAM

Modelling chemistry and transport in urban street canyons

Dai, Yuqing; Cai, Xiaoming; Zhong, Jian; MacKenzie, A. Robert

Link to publication on Research at Birmingham portal

1 **Modelling chemistry and transport in urban street canyons: Comparing**
2 **offline multi-box models with large-eddy simulation**

3 Yuqing Dai, Xiaoming Cai, Jian Zhong, A. Rob MacKenzie[*]
4 School of Geography, Earth & Environmental Sciences, University of Birmingham, Edgbaston,
5 Birmingham B15 2TT, UK

6
7 *Corresponding author

8
9 **AUTHOR EMAIL ADDRESSES:**
10 Yuqing Dai: yxd598@bham.ac.uk
11 Jian Zhong: j.zhong.1@bham.ac.uk
12 Xiaoming Cai: x.cai@bham.ac.uk [retired]
13 A. Rob MacKenzie: a.r.mackenzie@bham.ac.uk

14
15 Corresponding author:
16 A. Rob MacKenzie: a.r.mackenzie@bham.ac.uk; telephone: +44 0121 414 6142.

17 **Highlight**

18 • NO_x-O_3-VOC chemical reactions are coupled with multi-box canyon models.
19 • The multi-box models reproduce flow characteristics in regular and deep canyons.
20 • Reactive species concentrations in street canyons are well captured in <1% of the run
21   time of computational fluid dynamics.
22 • The impacts of segregation on reactive species can be investigated.

23 **Abstract**

24 Computational fluid dynamics models are resource-intensive, particularly when complex chemical
25 schemes are implemented, and this computational expense limits their use in sensitivity analyses. We
26 propose a flexible multi-box model that permits spatial disaggregation of sources and depositions to
27 simulate the transportation and distribution of chemical species in street canyons with any aspect
28 ratios for which a large eddy simulation (LES) of the flow exists. The spatial patterns of reactive
29 species in the multi-box simulations are in good agreement with those from the LES, especially for
30 the deep canyon from which air escapes more slowly. The overestimation of the LES simulation

31 worsens somewhat due to segregations when the chemistry of volatile organic compounds (VOCs) is
32 included but the overall pattern is captured in a modelling framework. By reducing computational
33 costs by several orders of magnitude, the multi-box model allows more sensitivity testing than the
34 LES, and is an effective approach to investigate spatial pattern of fast non-linear chemistry or
35 microphysics at the street scale.

36 *Keywords:* Air quality; Urban air pollution; Box models; Street canyon; Nitrogen dioxide; Ozone

37 **1. Introduction**

38 Street canyons typically combine to build up a semi-enclosed urban environment with high
39 concentrations of anthropogenic pollutants trapped inside, leading to persistent higher exposure risk
40 for pedestrians near the roadside (Ahmad et al., 2005; Oke, 1988; Vardoulakis et al., 2003). Canyons
41 can be divided into three types in terms of the ratio of building height (H) to street width (W), namely
42 aspect ratio (AR): wide canyons (AR < 0.3), regular canyons (AR ≈ 1), and deep canyons (AR > 1.3)
43 (Vardoulakis et al., 2003). Oke (1988) classified the canyon flows into three isothermal regimes
44 according to AR and L/W (L is the building length along the span-wise direction). These regimes
45 include skimming flow (0.66 < AR < 1.57), wake interference flow (0.1 < AR < 0.66) and isolated
46 roughness flow (AR < 0.1). Besides the isolated roughness flow, wake interference flow, and
47 skimming flow, there is the fourth flow regimes, i.e., multi-vortex flow regime in deep street canyons.
48 If Reynolds (Re) number independence is satisfied, there is only one-vortex when AR is 1 and 3, but
49 two main vortexes appear when AR is 5 or more (Yang et al., 2020). However, in wind-tunnel-scale
50 street canyons (H = 6 cm, Re~1.2×10^4), if Re number is not sufficiently large, there are two contra-
51 rotative vortices when AR = 2 and three to five vertically aligned vortices when AR is 3-5 (Li et al.,
52 2008). The main difference between these two groups is whether the requirement of Re-number
53 independence is satisfied or not. Chew et al. (2018) proposed that the widely adopted criterion Re >
54 11,000 for ensuring Reynolds-number-independence (Re-independence) is not applicable for 2D
55 street canyons as AR > 1.5. They discovered that only one primary vortex appeared when AR = 2 if
56 Re > 8.7×10^4. Moreover, Yang et al. (2021) found that isothermal urban airflows for full-scale deep
57 canyons can be independent of Re when Re exceeds 1×10^6 and 1×10^7 when AR is 3 and 5.

58 Because of much of the human exposure to outdoor air pollutants occurs at the pedestrian level in
59 street canyons, understanding airflow characteristics and distributions of pollutants is of vital

importance in evaluating the pollutant health risk and in making policy for targeted air pollution alleviation. The concentration of a passive scalar (PS, an idealised chemically inert substance that negligibly interferes with local fluid dynamics through effects such as buoyancy) can exhibit sharp gradients at the pedestrian level of the street canyons (Fellini et al., 2020; Lietzke and Vogt, 2013; Murena et al., 2009). Furthermore, the dispersion of atmospheric pollutants within the canyon is accompanied by complex non-linear chemical reactions, evolving on the timescale comparable to the canyon circulation and residence timescale. During the past two decades, studies have focused on the investigation of time-evolution and spatial variations of reactive species, for example, nitric oxide (NO), nitrogen dioxide (NO_2), and ozone (O_3) in street canyons, using coupled computational fluid dynamics (CFD) such as Reynolds-Averaged Navier-Stokes (RANS) and Large-Eddy Simulation (LES) models with different chemical schemes. Baker et al. (2004) integrated an LES model with a simple NO_x-O_3 cycle (two reactions in sunlight) to simulate the dispersion and spatial distribution of reactive species in a regular street canyon. The impacts of dynamics on the chemistry had been investigated by introducing the concept of the photo-stationary state defect (PSSD). Low PSSD values indicate equilibrium-like chemistry and were found at the centre of the primary vortex and on the windward corner at the street level. High PSSD values indicate rapidly-changing chemistry and were found at the location near NO_x sources, along the leeward facet (where pollutants were escaping the street canyon), and along the windward wall on the outer edge of the vortex (where fresh air was entrained into the canyon). Baik et al. (2007) adopted the renormalised k-ε RANS model coupled with the simple NO_x-O_3 photochemistry to simulate pollutant dispersion with the effects of street-bottom heating; Kwak and Baik (2012) further incorporated Volatile organic compounds (VOC) chemistry into the model and discussed the sensitivity of O_3 concentrations to NO_x and VOC emissions. Kim et al. (2012) examined reactive species in a regular canyon using RANS with a comprehensive tropospheric NO_x-O_3-VOC chemistry from GEOS-Chem. They found a substantial influence of different chemical schemes on O_3 levels and highlight the importance of more explicit chemistry simulation. However, Bright et al. (2013) found that VOCs could contribute additional but modest NO_2 and O_3 formation (about 12%) in the regular canyon, which is consistent with Garmory et al. (2009). Zhong et al. (2017) extended the LES model with the NO_x-O_3-VOC chemistry to simulate the spatial distribution of reactive species in an idealised deep urban street canyon. They revealed that volume-averaged NO_2 and the total oxidants (O_x) concentrations significantly increased due to VOCs-relating chemistry. Their works provided a better understanding of the combined effects of insufficient

91 mixing and non-linear reactions in street canyons with a higher aspect ratio. Zhang et al. (2020)

92 conducted RANS simulations with a simple NO_x-O_3 cycle in street canyons with AR = 1, 3 and 5, but

93 their work neglected the effect of organic free radicals, which is likely important in determining the

94 concentration of reactive species inside deep street canyons. Recently, Wu et al. (2021) developed a

95 platform that integrated a CFD model (i.e., OpenFOAM) and a photochemical mechanism including

96 VOCs for pollutant dispersion in the regular canyon. Although these CFD-based studies provide

97 promising methods in order to simulate physical dispersion and chemical transformation of reactive

98 species within canyons, modelling scenarios in reality are much more sophisticated in terms of, for

99 example, emissions (Wu et al., 2021), wind conditions, roof shapes (Takano and Moonen, 2013),

100 ground or wall heating (Cai, 2012), and the presence of green infrastructures such as trees with

101 varying leaf area density (Abhijith et al., 2017; Gromke et al., 2008; Gromke and Ruck, 2007). The

102 domain/model configurations need to be adjusted from case to case, and using a CFD model is, in

103 general, very computationally expensive for the study of such a wide range of scenarios, especially

104 when explicit VOC chemical reactions are included.

105 A more convenient and efficient way is adopting offline simulations, as is routinely employed at

106 regional and global scales (e.g., Jacobson and Jacobson (2005); Kukkonen et al. (2012)). The zero-

107 dimensional one-box model can easily adopt complex chemistry without intensive computational

108 resources. It also exhibited satisfactory performance compared to the LES (Bright et al., 2013),

109 despite relatively higher modelled NO, NO_2 and hydroxyl radical (OH) concentrations. Zhong et al.

110 (2016) implemented a coupled two-box model with NO_x-O_3-VOC chemistry for simulating pollutants

111 in a deep canyon. They highlight that the one-box treatment would miscalculate flow structure and

112 pollutant gradients, and, hence, underestimate the exposure risk of pedestrians to NO_2 in the deep

113 canyon. However, these simplified box models are still too coarse to evaluate air quality conditions

114 at the pedestrian level. They would systematically neglect substantial concentration contrasts near the

115 centre of the carriageway and cannot capture the horizontal distribution of pollutants, which is as

116 important as vertical features in street canyons. The lack of available process-based methods makes

117 it difficult to investigate systematically coupled chemistry-transport effects in street canyons.

118 In this study, a multi-box model with a flexible number of boxes and flexible chemical schemes has

119 been developed for air pollution simulations in street canyons. The model design, mathematical

120 formulation, and configurations for testing are described in Section 2. In Section 3, the modelling

121   results of reactive species from the multi-box models with a reduced NO_x-O_3-VOC chemistry and a
122   simple NO_x-O_3 cycle are evaluated against the published modelling data from the LES dynamical
123   models at the box grid resolution, for idealised regular and deep street canyons. The time-evolution
124   of concentrations, segregation effects due to overly fast chemistry in the multi-box case, and spatial
125   variations inside canyons are discussed in detail. The conclusions and future perspective are
126   summarised in Section 4. Although not the focus of the current paper, we note that aerosol
127   microphysics introduces non-linear processes in street canyons in a similar way to chemistry (Gelbard
128   and Seinfeld, 1980; Jacobson and Seinfeld, 2004; Jacobson et al., 1996; Zhong et al., 2020a, b; Zhong
129   et al., 2018); the modelling framework described below could be extended to include detailed size-
130   dependent aerosol microphysics in the future.

131   **2. Methods**

132   2.1. Description of models

133   2.1.1 The multi-box model

134   The principle of the multi-box model is to split the volume of street canyons into several boxes, where
135   each box ideally reflects a resolved airflow arising from the aspect ratio or physical obstructions in
136   street canyons (e.g., Fig. 1). In the two-dimensional framework, boxes inside the model are indexed
137   based on their locations in Cartesian coordinates. Assuming the background wind above the roof level
138   blows across the street canyon from left to right, starting from the bottom-left to the top-right, e.g.,
139    $Box_{[1,1]}$ represents the leeward corner of a canyon. Pollutant transfer between adjacent boxes is
140   determined by the mean wind advection and by turbulent diffusion across the mesh interface. Vertical
141   (denoted by capital "G") and horizontal (denoted by capital "F") mixing-ratio fluxes (ppb m s^{-1}) for
142   pollutant, q, into $Box_{[k,i]}$ (i.e., "k" represents vertical index position, "i" represents horizontal index
143   position) can be formulated as:

144    $$F_{e,[k,i]} = u_{e,[k,i]}\left(C_{q,[k,i-1]} - C_{q,[k,i]}\right)$$

    (1)

145    $$F_{a,[k,i]} = \begin{cases} U_{a,[k,i]}C_{q,[k,i-1]}, & U_{a,[k,i]} \geq 0 \\ U_{a,[k,i]}C_{q,[k,i]}, & U_{a,[k,i]} < 0 \end{cases}$$

    (2)

146 $$G_{e,[k,i]} = w_{e,[k,i]} \left(C_{q,[k-1,i]} - C_{q,[k,i]} \right)$$

(3)

147 $$G_{a,[k,i]} = \begin{cases} W_{a,[k,i]} C_{q,[k-1,i]}, & W_{a,[k,i]} \geq 0 \\ W_{a,[k,i]} C_{q,[k,i]}, & W_{a,[k,i]} < 0 \end{cases}$$

(4)

148 where $G_{a,[k,i]}$ (ppb m s^{-1}) and $F_{a,[k,i]}$ (ppb m s^{-1}) are mixing-ratio fractional fluxes due to advective

149 transfer (i.e., flow resolved by the LES); $G_{e,[k,i]}$ (ppb m s^{-1}) and $F_{e,[k,i]}$ (ppb m s^{-1}) are mixing-ratio

150 fluxes due to turbulent diffusion formulated by the Fick's law. $W_{a,[k+1,i]}$ (m s^{-1}) and $U_{a,[k,i+1]}$ (m s^{-1}) are

151 the advective transfer velocities in the vertical and horizontal directions, respectively; and $w_{e,[k+1,i]}$ (m

152 s^{-1}) and $u_{e,[k,i+1]}$ (m s^{-1}) are transfer velocities due to turbulent diffusion. By assuming all fluxes as

153 vectors with positive values along the coordinate directions, the concentration in Box$_{[k,i]}$ can be

154 calculated from the following equation:

155 $$\frac{dC_{q,[k,i]}}{dt} = E_{q,[k,i]} - \frac{G_{a,[k,i+1]} + G_{e,[k,i+1]}}{l_i} + \frac{G_{a,[k,i]} + G_{e,[k,i]}}{l_i} - \frac{F_{a,[k+1,i]} + F_{e,[k+1,i]}}{h_k} + \frac{F_{a,[k,i]} + F_{e,[k,i]}}{h_k} + \Delta S_{q,[k,i]} + \Delta V_{q,[k,i]}$$

(5)

156 where $C_{q,[k,i]}$ (ppb) is the mixing-ratio of the qth species in Box$_{[k,i]}$, $E_{q,[k,i]}$ (ppb s^{-1}) is the emission rate

157 of the qth species into Box$_{[k,i]}$, h_k (m) and l_i (m) are the box height and box width respectively, $\Delta S_{q,[k,i]}$

158 (ppb s^{-1}) is the net production rate of the qth species due to chemistry in Box$_{[k,i]}$, and $\Delta V_{q,[k,i]}$ (ppb s^{-1})

159 is the net deposition term of the qth species in Box$_{[k,i]}$. Allowing computations with more species, and

160 where the associated $\Delta S_{q,[k,i]}$ terms reflect more complicated non-linear chemistry, is one of the prime

161 motivations for the development of the box model. By default, the boundary layer above the street

162 canyon is assumed as one compartment, representing relatively steady background conditions over a

163 long period (e.g., 1 hour). The 4th order Runge-Kutta method is adopted in the multi-box model to

164 solve the ordinary differential equations (ODEs) numerically. To facilitate a systematic investigation,

165 we use two dimensionless ratios to represent the size of grid boxes to the entire street canyon:

166 $$\alpha_k = \frac{h_k}{h_0}$$

(6)

167 $$\beta_i = \frac{l_i}{l_0}$$

(7)

168   where h_0 (m) and l_0 (m) are the canyon height and street width, respectively. Then the volume-

169   averaged concentrations of qth species ($C_{q,m\times n\text{-box}}$) for the entire canyon with m × n boxes is:

$$C_{q,m\times n\text{-box}} = \sum_{k=1;i=1}^{k=m;i=n} \alpha_k \beta_i C_{q,[k,i]}$$

170   (8)

171   If the volume is equal for all the boxes in street canyons, that is, i.e., $\alpha_1 = \alpha_2 = ... = \alpha_k = \dfrac{1}{m}$ and

172     $\beta_1 = \beta_2 = ... = \beta_i = \dfrac{1}{n}$, then the equation (8) can be rewritten to:

$$C_{q,m\times n\text{-box}} = \frac{\sum_{k=1;i=1}^{k=m;i=n} C_{q,[k,i]}}{m \times n}$$

173   (9)

174   Additionally, a dimensionless factor $\gamma_{q,[k,i]}$ is adopted to account for the heterogeneous on-road

175   emission of the qth species:

$$\gamma_{q,[k,i]} = \frac{\alpha_k \beta_i E_{q,[k,i]}}{\sum_{k=1;i=1}^{k=m;i=n} \alpha_k \beta_i E_{q,[k,i]}}$$

176   (10)

177   Up to n continuous line sources could be added into the kth (k = 1, 2, …, m) layer of the canyon, which

178   is helpful for elevated road or rail sources and for biogenic emissions from street trees. $\gamma_{q,[k,i]} = 0$ or

179     $\gamma_{q,[k,i]} = 1$ indicates that no emission or all vehicle emissions have been injected into $Box_{[k,j]}$.

180   In order to derive net chemical terms especially for short-lived reactive species such as hydroxyl

181   radical (OH) and hydroperoxyl radical (HO_2), the ODEs of a chemical system for q^{th} species can be

182   written as:

$$\frac{d}{dt}C_{q,[k,i]} = P_{q,[k,i]} - L_{q,[k,i]}C_{q,[k,i]}$$

183   (11)

184   where $P_{q,[k,i]}$ and $L_{q,[k,i]}$ are the chemical production and loss rates in the specific $Box_{[k,i]}$. If those

185 chemical kinetics remain constant during a given timestep, Δt, equation (11) may be solved

186 numerically with the quasi-steady-state approximation (QSSA):

$$C_{q,[k,i],t_0+\Delta t} = \frac{P_{q,[k,i],t_0}}{L_{q,[k,i],t_0}} + \left(C_{q,[k,i],t_0} - \frac{P_{q,[k,i],t_0}}{L_{q,[k,i],t_0}} \right) e^{-L_{q,[k,i],t_0}\Delta t}$$

187 (12)

188 where t_0 represents the starting point of each time interval during simulations. The chemical lifetime

189 of qth species, $\tau_{q,[k,i]}$, in the Box$_{[k,i]}$ is:

$$\tau_{q,[k,i]} = \frac{1}{L_{q,[k,i]}}$$

190 (13)

191 If $\tau_{q,[k,i]} < 0.1\Delta t$, chemical reactions are extremely fast compared to Δt, which means the chemical-

192 steady-state can be adopted:

$$C_{q,[k,i],t_0+\Delta t} = \frac{P_{q,[k,i],t_0}}{L_{q,[k,i],t_0}}$$

193 (14)

194 If $\tau_{q,[k,i]} > 100\Delta t$, chemical reactions take through much slower compared to Δt, and the forward

195 Eulerian formula can be used:

$$C_{q,[k,i],t_0+\Delta t} = C_{q,[k,i],t_0} + \left(P_{q,[k,i],t_0} - L_{q,[k,i],t_0} C_{q,[k,i],t_0} \right) \Delta t$$

196 (15)

197 If $0.1\Delta t < \tau_{q,[k,i]} < 100\Delta t$, then the chemical timescale has a comparable magnitude with Δt, and

198 equation (12) is employed for the calculation. However, solving equation (12) incurs substantial

199 computational costs in practice. Alexandrov et al. (1997) proposed an alternative way for the

200 optimisation of the QSSA algorithm, which rationally expands the exponential term based on the

201 Taylor expansion in the second order:

$$e^{-L_{q,[k,i],t_0}\Delta t} \approx \frac{1}{1 + L_{q,[k,i],t_0}\Delta t + 0.5(L_{q,[k,i],t_0}\Delta t)^2}$$

202 (16)

203 and equation (12) can be reformatted as:

$$C_{q,[\mathrm{k,i}],t_0+\Delta t} = \frac{C_{q,[\mathrm{k,i}],t_0} + \left(1 + 0.5 L_{q,[\mathrm{k,i}],t_0}\Delta t\right) P_{q,[\mathrm{k,i}],t_0}\Delta t}{1 + L_{q,[\mathrm{k,i}],t_0}\Delta t + 0.5(L_{q,[\mathrm{k,i}],t_0}\Delta t)^2}$$

204

(17)

205　In the one- and multi-box models, reactive species have been divided into two categories in terms of

206　their chemical lifetime. For the regular and deep canyons, an empirical timestep value of 0.03 s was

207　used with equation (15) for numerical integration of long-lived species (e.g., NO, NO_2, O_3), and a

208　value of 0.003 s with the equation (17) was used for short-lived species (e.g., HO, HO_2). They are the

209　same as those used in the LES (Bright et al., 2013; Zhong et al., 2015) based on the timescale of the

210　turbulent eddies, which also indicates that no species are fully in steady state in urban street canyon

211　environment.

212　The multi-box model is written in R version 3.6.2 (R Core Team, 2019) and Fortran 90 (using the

213　Intel Fortran (IVF) Compiler) in the origin version 1.0, including three modules: the main program,

214　the dynamical submodule, and a chemical submodule. Modularisation allows the model to be easily

215　modified or updated for various research purposes, e.g., to investigate the impact of different chemical

216　mechanisms on air quality in street canyons or to investigate in-canyon particle microphysics (cf.,

217　Nikolova et al. (2016)).

218　Additionally, a typical one-box model is used as a reference in this study, and the mathematical

219　expression is (Liu and Leung, 2008):

$$\frac{dC_{q,0}}{dt} = E_{q,0} - \frac{w_{t,0}}{h_0}\left(C_{q,0} - C_{q,b}\right) + \Delta S_{q,0} + \Delta V_{q,0}$$

220

(18)

221　where a subscript "0" indicates that signs have the same meaning as those in the multi-box model but

222　for a whole space of the street canyon in volume. The parameter $w_{e,0}$ (m s^{-1}) represents the "exchange

223　velocity" between the street canyon and boundary layer above the rooftop. A two-box model is also

224　used only for simulations in the deep street canyon, the mathematical expressions are (Murena, 2012;

225　Zhong et al., 2016):

$$\frac{dC_{q,\mathrm{L}}}{dt} = E_{q,\mathrm{L}} - \frac{w_{t,\mathrm{L}}}{h_\mathrm{L}}\left(C_{q,\mathrm{L}} - C_{q,\mathrm{U}}\right) + \Delta S_{q,\mathrm{L}} + \Delta V_{q,\mathrm{L}}$$

226

(19)

$$\frac{dC_{q,U}}{dt} = \frac{w_{t,L}}{h_U}\left(C_{q,L} - C_{q,U}\right) - \frac{w_{t,U}}{h_U}\left(C_{q,U} - C_{q,b}\right) + \Delta S_{q,U} + \Delta V_{q,U}$$

227

(20)

228   where subscripts "L" and "U" indicate that signs have the same meaning as aforementioned but for

229   the lower and upper compartments (i.e., including 16 boxes in the red box to solve the main vortexes)

230   of the deep street canyon in volume, respectively. $w_{e,L}$ (m s^{-1}) represents the "exchange velocity"

231   between two in-canyon compartments, and $w_{e,U}$ (m s^{-1}) represents the "exchange velocity" between

232   the upper compartment and the overlying background.

233   2.1.2 Large-eddy simulation

234   The LES results of reactive species were taken from Bright et al. (2013) for an idealised regular

235   canyon, and from Zhong et al. (2017) for a deep canyon. Their studies applied OpenFoam v2.1.1

236   (Jasak et al., 2007) to resolve turbulence at large spatial and temporal scales and to simulate

237   incompressible airflow with a high Reynolds number (Re $\sim 1\times10^6$) in street canyons under the neutral

238   atmosphere. The unresolved sub-grid scales (SGS) processes were treated using the one-equation

239   SGS turbulence model, and the logarithmic law of the rough-wall (Schlichting and Gersten, 2016)

240   was used for the near-wall treatment. Symmetry boundary conditions were used for the domain

241   overlying the canyon, and cyclic boundary conditions were employed in x- and y-directions. A

242   constant pressure gradient in the upper background was assumed to produce a flow perpendicular to

243   the canyon axis. The simulations of the LES were conducted with only dynamics for about 5 h in

244   order to obtain a dynamical-steady flow field, which was further adopted as the initial turbulence

245   condition.

246   For the regular canyon, the resolved turbulent kinetic energy (TKE) has been evaluated against wind-

247   tunnel experiments (Cui et al., 2004) and the scalar has been validated by Cai et al. (2008); for the

248   deep canyon, the flow field agreed well with water-channel (Li et al., 2008) and wind tunnel (Kovar-

249   Panskus et al., 2002) experiments. The deposition of air pollutants is not considered in the LES

250   modelling. The method for integrating VOC chemistry in the LES modelling is similar to that of the

251   multi-box simulations described above and has been detailed in Zhong et al. (2017). The methods for

252   initialising and processing the LES (e.g., emission, time step) are also adopted directly for the multi-

253   box model and are described in the following section.

254 2.2. Model configurations

255 2.2.1 Street canyon geometry

256 The LES domains adopted for regular (AR = 1) and deep (AR = 2) canyons were presented in Fig.
257 1(a) and Fig. 1(b), respectively. In the LES, mesh resolutions were 0.3 m, 1.0 m and 0.3 m in the x,
258 y, z directions, respectively, inside street canyons. That is, there are respectively 3,600 and 7,200 cells
259 inside regular and deep canyons in the LES simulations. For the layer above the canyon in the LES
260 simulation, Δz gradually increased by a factor of 1.15 from the rooftop to the domain top (z_0 = 18-90
261 m and z_0 = 36-112 m for regular and deep canyons). Fig. 1(c) and Fig. 1(d) are the respective
262 counterparts in multi-box models for the cross-section canyons. The building height and street width
263 are 18 m ($h_0 = l_0$) for the regular street canyon, and are 36 and 18 m ($h_0 = 2l_0$) for the deep street
264 canyon. The red frame in Fig. 1(d) presents a two-box model with $h_L = h_U = 18$ m. One primary
265 clockwise vortex forms in the simulations of the regular canyon as the background skimming wind
266 perpendicularly blows along the x-direction across the canyon axis; however, in the deep street
267 canyon, a clockwise vortex in the upper compartment and a weak counter-clockwise vortex in the
268 lower compartment are formed. In the multi-box model, the in-canyon volumes have been divided
269 into identical 16 and 32 boxes for the regular and deep canyons, respectively (namely the 16- and 32-
270 box models). This implies that each grid has a volume of 4.5 m $\times$ 1 m $\times$ 4.5 m = 20.25 m^3.

271 2.2.2 Dynamical parameters for air mass exchange

272 The exchange velocity ($w_{e,0}$) for the one-box model, and the advective and turbulent velocities for the
273 multi-box model, are of the utmost importance in determining the intensity of in-canyon mixing, and
274 transport and rates of escape of atmospheric pollutants to the overlying background. The values of
275 $w_{e,0}$ = 0.022 m s^{-1} and $w_{e,0}$ = 0.012 m s^{-1} are respectively adopted for the cross-section 18 m $\times$ 18 m
276 regular and 18 m $\times$ 36 m deep canyons (as in Fig. 1) in the one-box model, corresponding to a
277 reference wind velocity of 2 m s^{-1} in the above rooftop layer under the neutral conditions (Cai, 2012a;
278 Zhong et al., 2017). The values of $w_{e,L}$ = 0.0229 m s^{-1} and $w_{e,U}$ = 0.0156 m s^{-1} are used for the two-box
279 simulation in the deep canyon, respectively.

280 In order to quantify the transport due to advection ($W_{a,[k,i]}$ and $U_{a,[k,i]}$, denote "advective velocities"
281 in this study) and mixing due to turbulence ($w_{e,[k,i]}$ and $u_{e,[k,i]}$, denote "turbulent velocities") in the

282   multi-box model, firstly vertical mixing-ratio fluxes including advective fluxes and turbulent fluxes

283   of PS at the interface of boxes were extracted from the LES modelling results, and the averaged values

284   over a period of the last 60 minutes were used for calculations. The total horizontal fluxes were then

285   derived based on the flux balance of each grid on the Eulerian coordinates under an assumed

286   equilibrium state over the period. These LES-derived fluxes describe the transmission of PS between

287   any two adjacent boxes in street canyons. However, the velocities from the LES simulations

288   (representing "real" wind conditions) cannot be used directly, because they need to be adjusted to

289   calculate the mass transfer between coarser grids. Therefore, pollutant advective velocities ($U_{a,[k,i]}$ and

290    $W_{a,[k,i]}$) are obtained using the vertical advective fluxes ($F_{a,[k,i]}$ and $G_{a,[k,i]}$) and the grid concentrations

291   (i.e., an volume-averaged value at the grid resolution of the multi-box model) following Equation (2)

292   and (4), and vertical mixing-ratio turbulent velocities ($w_{e,[k,i]}$ and $u_{e,[k,i]}$) are obtained using vertical

293   turbulent fluxes ($F_{e,[k,i]}$ and $G_{e,[k,i]}$) and concentration gradients based on Equation (1) and (3). In this

294   way, the mass fluxes of the multi-box and LES models are consistent at the same box interface under

295   the equilibrium state. It is noted that the derivation for horizontal fluxes may have uncertainties

296   because emissions from a single line source are simply assumed to be injected into one grid in the

297   multi-box model, whereas a Gaussian distribution over the carriageway was assumed in the LES

298   model. A coarser grid resolution can reduce this type of error. Therefore, in this study, the 16- and

299   32-box models are used to evaluate reactive species in regular and deep urban street canyons, and the

300   details of advective and turbulent velocities are presented in the support information (Table S1 and

301   Table S2). Model performance under higher horizontal resolutions is left to be evaluated in future

302   work.

303   Due to the very similar magnitude of advective fluxes entering and escaping the street canyon in the

304   neutral atmosphere (Salizzoni et al., 2009), the escaping canyon fluxes due to vertical advection are

305   rotated into the horizontal direction, and thus the multi-box model considers only turbulent terms at

306   the rooftop. Turbulent velocities as described above could be negative (although usually of small

307   magnitude in such cases), indicating counter-gradient turbulent diffusion under the box-model

308   framework (Figs. 1c and 1d). This may cause the model to crash during a box model timestep if

309   concentrations become negative. In order to address this issue, a minimum positive value of 1.0×10^{-4}

310   m s^{-1} is applied to the turbulent velocity, implying a very small turbulent flux compared to the

311   advective flux for the interface under such conditions.

312   2.2.3 Emissions and chemical mechanism

313   Traffic-related pollutants were emitted by two consecutive line-sources at 1 m height and at 2.5 m to
314   the left and right of the street centre axis for the LES models. Therefore the emissions were evenly
315   injected into $Box_{[1,2]}$ and $Box_{[1,3]}$ at the street level for the multi-box models ($\gamma_2 = \gamma_3 = 0.5$). The
316   emission rates of NO, NO_2, carbon monoxide (CO), ethene (C_2H_4), propene (C_3H_6), formaldehyde
317   (HCHO) and acetaldehyde (CH_3CHO) were calculated based on the UK Road Vehicle Emission
318   Factors (Boulter et al., 2009), which were 558, 62, 1356, 56, 24, 32 and 15 g km^{-1} hr^{-1}, representing
319   a typical weekday traffic scenario of 1500 vehicles per hour with an average speed of 30 miles per
320   hour (mph), which equate to 900, 100, 3593, 347, 150, 96 and 98 ppb s^{-1} for the LES cell; to 4.0, 0.44,
321   16, 1.55, 0.67, 0.88 and 0.42 ppb s^{-1} for the 16- (and 32-) box grid; and to 0.252, 0.028, 1.0, 0.097,
322   0.042, 0.055 and 0.026 ppb s^{-1} for the one-box grid in the regular canyon and for the two-box grid in
323   the deep canyon. Moreover, PS that only undergoes physical processes was injected at the same rate
324   with NO_x (= NO + NO_2) to investigate the sole effect of canyon dynamics on the model performance.

325   The Reduced Chemical Scheme (RCS) was developed by Bright et al. (2013), based on the Common
326   Representative Intermediates mechanism version CRI *v2-R5* (Watson et al., 2008). The RCS retains
327   the compounds that have important effects on core chemical intermediates in urban street canyons
328   and includes 51 gas-phase species and 136 chemical reactions. The chemical kinetics are calculated
329   at 20°C under a standard atmosphere pressure (e.g., photodegradation rate of 9.20×10^{-3} s^{-1} for NO_2),
330   and they are adopted for simulating the daytime chemistry in the present study. The comparison
331   between RCS and the benchmark Master Chemical Mechanism (12691 chemical reactions of 4351
332   species for MCM*v3.0*) (Saunders et al., 2003) showed that the maximum differences were 3%, 13%,
333   16%, and 12% for NO, NO_2, O_3 and OH during a four-hour simulation, which was comparable to, or
334   smaller than, the errors from emissions and detection techniques (Boulter et al., 2009; Heard and
335   Pilling, 2003). The total computation time of the multi-box model with RCS is about 6 minutes, which
336   is higher than that of the one-box (~1 s) and two-box models (~8 s), but is significantly faster
337   compared to those of the LES (around 10 days) (Zhong et al., 2017).

338   2.2.4 Model initialisation and output post-processing

339   The initial concentrations of the multi-box model are consistent with those in LES conditions for two
340   types of canyons, which were taken from the field study of the Tropospheric Organic Chemistry

341   (TORCH) experiment (Lee et al., 2006). These observations represent a typical atmospheric condition

342   in rural London, UK, during the summer of 2003. The models have been operated for 30 min "spin-

343   up" period without any emission in order to initialise the chemical intermediates, then traffic

344   emissions are switched on and concentrations of all species at $t = 30$ min are used as the cyclic "fixed"

345   background conditions for a next 210 min modelling duration (i.e., $t = 30\text{-}240$ min) in a time step of

346   0.03 s. The solar radiation intensity remains constant during the model operation. "*zero background*"

347   for PS is assumed during the LES and box operations.

348   The concentrations from box models were stored in an interval time step of 1 min for time-evolution

349   analysis. The final hour of the modelling results (i.e., $t = 180\text{-}240$ min) was extracted for the

350   calculation. Details about LES outputs pre-processing can be found in Bright et al. (2013) (for the

351   regular canyon) and Zhong et al. (2015) (for the deep canyon), respectively. Subsequently, the

352   modelling results of LES were averaged equivalent to the coarse resolution of box models for the

353   purpose of evaluating the spatial distributions of air pollutants with the multi-box models. In order to

354   investigate the impacts of incomplete mixing on the sub-grid scale variability due to chemistry, a

355   widely-used dimensionless parameter *intensity of segregation* (Krol et al., 2000) is adopted in this

356   study:

357
$$I_{S(q_1+q_2)} = \frac{\left\langle q_1^* q_2^* \right\rangle}{\left\langle q_1 \right\rangle \left\langle q_2 \right\rangle}$$
(21)

358   where $I_{S(q_1+q_2)}$ represents the intensity of segregation between chemical species q_1 and q_2, angle

359   brackets refer to the volume-averaged conservation quality, defined by Equation (8) for the multi-box

360   model, $<q_1^* q_2^*>$ represents the volume-averaged covariance between q_1 and q_2, and an asterisk means

361   the deviation from the averaged value. So, for a general case, we have $\left\langle q_1 \right\rangle = \sum \alpha_k \beta_i C_{q_1,[k,i]}$,

362    $\left\langle q_2 \right\rangle = \sum \alpha_k \beta_i C_{q_2,[k,i]}$, $q_{1,[k,i]}^* = C_{q_1,[k,i]} - \left\langle q_1 \right\rangle$, $q_{2,[k,i]}^* = C_{q_2,[k,i]} - \left\langle q_2 \right\rangle$, and $\left\langle q_1^* q_2^* \right\rangle = \frac{1}{16} \sum q_{1,[k,i]}^* q_{2,[k,i]}^*$. The

363   volume-averaged second-order reaction rate ($<k_{(q_1+q_2)}>$) can be written as:

364
$$\left\langle k_{(q_1+q_2)} \right\rangle = k_{(q_1+q_2)} \left(1 + I_{S(q_1+q_2)} \right)$$
(22)

365   where $k_{(q_1+q_2)}$ is the original reaction rate in the sufficiently well-mixed one-box model. Therefore,

366     $I_{S(q_1+q_2)}$ can also be thought of as quantifying the deviation from chemical equilibrium due to the

367   spatial segregation associated with atmospheric dynamics. For any species in the one-box model,

368     $I_{S(q_1+q_2)}$ equals to zero because there is no spatial segregation inside the box. A positive $I_{S(q_1+q_2)}$

369   indicates that $<k_{(q_1+q_2)}>$ in the 16-box model is larger than $k_{(q_1+q_2)}$ in the one-box model because of the

370   segregation effect. When $q_1 = q_2$, $I_{S(q_1+q_2)}$ represents the spatial variability of any specific pollutant in

371   respect to its canyon volume-averaged concentration.

372   **3. Results and discussion**

373   3.1. Temporal evolution and the intensity of segregation within the canyon

374   Fig. 2 shows temporal evolution of the volume-averaged pollutant mixing-ratios of the LES, and

375   multi- and one-box models under the same raw emissions, meteorological conditions, and RCS

376   chemistry as the LES model, in idealised regular (a, b) and deep (c, d) street canyons, respectively.

377   Modelling results of the two-box model are available only for the deep canyon. The LES-RCS data

378   for the regular and deep canyons are from Bright et al. (2013) and Zhong et al. (2017), respectively.

379   The box models produce less temporal variability; reactive species slowly move toward a chemical-

380   transport equilibrium. The O_3 concentrations drop sharply after zero-emission "spin-up" period due

381   to NO and O_3 titration, accelerating the formation of NO_2 in street canyons. The OH and HO_2

382   concentrations rapidly relax to equilibrium when traffic emissions are switched on, the maintenance

383   of a steady-state HO_2 by oxidation of VOCs contributes to an additional NO_2 fraction. The chemical

384   species in the regular canyon achieve a transport-chemistry balance more quickly (i.e., about 90 min

385   for NO and NO_2) than in the deep canyon (e.g., around two hours for NO and NO_2) in both one- and

386   multi-box models, and the LES, because of more effective ventilation for canyons with a lower AR.

387   The concentrations of selected species at the equilibrium state over the final hour of model operation

388   are discussed below for a better understanding of the coupled dynamical and chemical processes in

389   street canyons.

390   Table 1 illustrates the time-averaged mixing-ratios of PS, NO, NO_2, O_3, OH, HO_2, NO_x (= NO +

391   NO_2), O_x (= NO_2 + O_3) and NO_2/NO ratios from the models coupled with the RCS chemistry during

392   the final simulation period ($180 \leq t \leq 240$ min) in the regular and deep street canyons, respectively.

393 For the regular canyon, LES outputs are slightly different from those in Bright et al. (2013), because
394 of the dynamics-driven variability in concentrations and the difference in averaging times (i.e., $180 \leq$
395 $t \leq 240$ min in the current study vs. $150 \leq t \leq 210$ min). The modelled mean PS concentrations of box
396 models are in good agreement with those of the LES-based models (differences within ±0.5%). The
397 spatially-averaged NO concentrations over the canyon are underestimated up to 4% by the box
398 models, while levels of other species are all overestimated to different extents, in particular with OH
399 levels (overestimated up to around 38%). The overestimations of O_3 are about 5.7% and 2.8% by the
400 one- and 16-box models compared to more accurate LES modelling results.

401 Previous modelling results (Bright et al., 2013) showed that the NO_x modelled by the zero-
402 dimensional one-box model were about 8 ppb (3.3%) higher than by the LES, O_3 concentrations were
403 underestimated by 6%, and NO was overestimated by around 1%. One explanation for the difference
404 between the results of the, present study and the previous study is that the value of $w_{e,0}$ adopted for
405 representing the canyon ventilation is ~5% higher in this study (i.e., $w_{e,0} = 0.22$) compared to their
406 work (i.e., $w_{e,0} = 0.21$), resulting in a higher abundance of O_3 in the street canyon due to inward
407 transport in from the background. The NO and NO_2 concentrations would be changed accordingly. It
408 should be noted that NO_x increases by about 1.6% in the box models, which means NO_x loss processes
409 (e.g., production of nitric acid and organic nitrates) are more effective in the LES model. The O_x
410 levels are respectively 9.0% and 11.1% higher in the 16- and one-box models because the efficient
411 mixing of background O_3 and in-canyon NO produces more NO_2 than under less efficient mixing
412 conditions, which is further discussed in the following section.

413 For the deep canyon, it is noted that the coarse resolution leads to a systematic underestimation of
414 about 3.0% in PS by the one-box model and of about 2% by the two-box model (Table 1); additionally,
415 Table 2 presents the mixing-ratio of pollutants from the LES, 32-box and two-box models in the upper
416 and lower compartments of the deep canyon, respectively. The 32-box model performs better than
417 the two-box model in simulating PS in both compartments. This may be attributed to the definition
418 of the exchange velocity (e.g., $w_{e,0}$, which is calculated based on the gradient between the whole
419 canyon-averaged and the ambient concentrations) and other dynamical parameters. For example, the
420 exchange velocities for the two-box and multi-box models are calculated based on the gradient
421 between the concentrations in the rooftop boxes and the overlying background. This more local

422   concentration gradient provides a better description for the flux balance in the multi-box model and

423   thus, better modelling results (i.e., closer to the LES outputs).

424   The difference in the flux-balanced exchange velocities may also have important impacts on the

425   chemistry in the canyon. The multi-box models include horizontal transport that can compensate

426   errors in modelling the canyon-averaged concentration, as less PS levels (around 1.5%) are

427   underestimated by the 32-box model. The box models overestimate reactive species except for NO

428   compared to the LES, which is consistent with the tendencies in the regular canyon. The absolute

429   errors between the LES and box models are larger for NO, NO_2 and O_3 but are smaller for OH and

430   HO_2 in the deep canyon, partly due to poor ventilation. Moreover, different chemical regimes may

431   exist in the canyon in terms of multi-vortices formed in the canyon, generating a complex outcome

432   for the whole-canyon averages. O_x is overestimated, as in the regular canyon, but NO_x is

433   underestimated partly because of the advective and turbulent velocities used in the model. The

434   concentration differences show a consistent pattern going from the complete-mixing (i.e., one-box

435   resolution) to resolved transport-and-mixing (i.e., LES resolution) conditions for most reactive

436   pollutants. That is, the multi-box model in general presents closer-to-LES results than the one-box

437   model. For example, instant mixing in street canyons accelerates more NO conversion to NO_2. Hence,

438   NO_2 is overestimated around 13% by the one-box model but 10% by the 16-box model in the regular

439   canyon; and it is overestimated about 15% by the one-box model, 13.6% by the two-box model, but

440   8.6% by the 32-box model in the deep canyon (Table 1 and 2). The NO_2/NO ratios gradually reduce

441   from 0.53 to 0.45, and from 0.63 to 0.47 in the regular and deep street canyons from the one-grid

442   approximation to the highest resolution, respectively. For the modelled concentrations of HO_x (= OH

443   + HO_2), the results of all the box models are very close to each other. The rationale behind this

444   similarity is discussed below using the intensity of segregation.

445   Table 3 compares the percentage intensities of segregation between any two selected chemical species

446   from the LES and multi-box models in regular and deep street canyons. It shows that the most

447   spatially variable air pollutant in the canyon is NO (i.e., indicated by $I_{S(NO+NO)}$) and the least spatially

448   variable pollutant is OH (i.e., indicated by $I_{S(OH+OH)}$) in general. Not surprisingly almost all intensities

449   of segregation in the deep street canyon are considerably higher (e.g., 26% for $I_{S(NO+NO)}$) than those in

450   the regular canyon (e.g., 3% for $I_{S(NO+NO)}$), which are supported by Zhong et al. (2017). It indicates

451   that NO concentrations become more heterogeneous due to the perturbed in-canyon vortexes, but OH

452   is less affected in terms of their abundance and lifetime in street canyons. It is also found that within

453   both types of canyons the values of $I_{S(q_1+q_2)}$ in the multi-box models mostly have a same sign with

454   those in the LES, which is positive for "emitted-inside-canyon" species (i.e., NO, NO$_2$) and is negative

455   for "entrained-from-background" and "formed in situ" species (i.e., O$_3$, OH, HO$_2$), indicating similar

456   chemical behaviours (e.g., generation or depletion) of these species in the LES and multi-scale models.

457   For atmospheric pollutants that directly react with each other, the intensities of segregation of the

458   multi-box models have a trend toward "zero" compared with the LES. For example, NO and O$_3$

459   titration rates are slower by 2.79% and 10.02% in regular and deep canyons under the "true" condition,

460   but slower by only 1.34% and 9.35% respectively under the "multi-box" approximation at the current

461   resolution. That is, the performance of multi-box model is in between the LES (i.e., close to the "true"

462   flow, insufficient mixing with hundreds of thousands of boxes) and the one-box model (i.e., instant

463   and homogeneous mixing with no segregation). On the contrary, the reactions of O$_3$ and HO$_2$

464   producing OH have been accelerated by 1.74% and 2.36% in the LES, but only by 0.42% and 1.56%

465   in the multi-box models.

466   3.2. The spatial variation of pollutants in street canyons

467   Fig. 3 illustrates vertical profiles ($0 < z/l_0 < 0.25$, $0.25 < z/l_0 < 0.5$, $0.5 < z/l_0 < 0.75$, $0.75 < z/l_0 < 1.0$)

468   of time-averaged PS, NO, NO$_2$, O$_3$, OH and HO$_2$ in the regular canyon (black lines), along with the

469   leeward (blue lines) and windward walls (red lines) in order to further ascertain the performance of

470   the multi-box model. In order to compare the model performance of the LES and multi-box model at

471   the same grid resolution, the quantities of the LES were averaged over the entire street width ($-0.5 <$

472     $x/l_0 < 0.5$) and the nearest box grid resolution adjacent to the canyon walls (i.e., $-0.5 < x/l_0 < -0.25$ for

473   the leeward, $0.25 < x/l_0 < 0.5$ for the windward), respectively. The distributions of chemical species

474   from the 16- and 32-box models are presented in the support information. Over the final hour of the

475   simulation, it is clear that the vertical distributions of PS from the 16-box model are in good agreement

476   (within 5 ppb) with those from the LES, with higher concentrations elevated on the leeward side of

477   the street corner (305.0 ppb) and considerably lower concentrations on the windward side (172.2 ppb)

478   due to the in-canyon air circulation. The agreement for PS indicates that the multi-box model with

479   LES-driven dynamics captured the major flow pattern well (i.e., a primary vortex) within the regular

480   street canyon.

481   The agreement for PS also implies that the discrepancies in the abundance of reactive species between

482   the multi-box and the LES models are mainly attributed to NO_x-O_3-VOC chemical reactions, though

483   their vertical and horizontal features are also well-reproduced by the multi-box model. NO

484   concentrations are well-simulated in $Box_{[1,4]}$ (difference within 1 ppb) but are slightly underestimated

485   at other grid points, especially for the leeward side (difference around 8 ppb, ~3%). Due to less

486   segregation for the 16-box model, there is a more effective O_3 titration in the canyon, which depletes

487   more NO turning to NO_2, thus causing an underestimation of NO and an overestimation of NO_2

488   contents in the 16-box model. Errors in NO_2 concentrations become smaller on the windward side but

489   become larger on the leeward side from the street level to the canyon rooftop. The maximum

490   overestimation of NO_2 is 15.6 ppb (19.1%) at $0 < z/l_0 < 0.25$ of the leeward side ($Box_{[1,1]}$) and 9.9 ppb

491   (12.6%) at $0.5 < z/l_0 < 0.75$ of the windward side ($Box_{[3,4]}$). The O_3 concentrations are underestimated

492   on the windward side with the maximum box-minus-LES value of 2.2 ppb (24.3%) at $0 < z/l_0 < 0.25$

493   ($Box_{[1,1]}$) due to effective titration with recirculated NO under the sufficient mixing condition.

494   However, there is an clear overestimation in O_3 contents on the leeward side with the maximum

495   difference of -3.6 ppb (19.1%) at $0.75 < z/l_0 < 1.0$ ($Box_{[1,4]}$). The explanation could be that more O_3

496   accumulated on the leeward side because of the rapid photodegradation of overproduced NO_2 due to

497   segregation effects on the windward side. Moreover, higher O_x levels in the 16-box model may be

498   attributed to overestimated HO_x concentrations (about 0.03 ppt for OH, 0.07 ppt for HO_2) in the street

499   canyon.

500   The Damköhler number (Da) is a widely used ratio of the chemical reaction rate to the diffusion rate

501   (or, equivalently, the ratio of diffusion timescale to reaction timescale) for determining the importance

502   of segregation effects on reactive species (Driscoll et al., 1992). If Da << 1, the dynamics achieve

503   "equilibrium" much faster than the reaction, leading to minimal segregation effects for the pollutant;

504   if Da >>1, the reaction may be considered to reach equilibrium instantaneously compared to the

505   relatively slower diffusion rates. That is, dynamics for the pollutants with substantial segregation

506   effects must be considered in a coupled manner (Garmory et al., 2006). Zhong et al. (2017) reported

507   the Da numbers of NO, NO_2, O_3, OH and HO_2 in the street canyon, which were 3.4, 5.8, 69, 1.44×10^5

508   and 4.44×10^4, respectively. The chemical reaction rates of HO_x are much quicker than the diffusion

509   rates across the model grid (Da >> 1). This explains that HO_2 is 0.02 ppt higher on the windward side

510   compared to the leeward side, and vertical distributions of OH and HO_2 from the 16-box model are
511   not significant compared to the outputs of the LES.

512   Fig. 4 shows the vertical distributions of selected species in the deep canyon and along with the
513   leeward and windward facets. The PS concentrations of the 32-box model are well-matched to those
514   of the LES model in both vertical and horizontal directions, with an underestimation of around 10
515   ppb (2.4%) on the leeward side and of 25 ppb (2.5%) on the windward side. Cumulative traffic
516   emissions produce very high PS mixing-ratios in the lower part of the canyon ($0 < z/l_0 < 1.0$). The
517   concentration of PS decreases smoothly with height on the leeward side but sharply varies on the
518   windward side, e.g., concentrations are higher on the windward side when $0 < z/l_0 < 1.0$ but on the
519   leeward side when $1.0 < z/l_0 < 2.0$. This indicates noticeable segregation between the lower and upper
520   compartments of the deep street canyon due to the presence of two counter-rotating vortices that are
521   captured by the LES and multi-box models. The upper vortex is driven by the ambient wind in the
522   shear layer at the rooftop ($z/l_0 = 2.0$) so that the characteristics of the vertical profiles are similar to
523   those of the regular canyon, while the lower vortex is driven by the upper vortex at approximately z/l_0
524    $= 1.0$ (or slightly lower) (Eliasson et al., 2006; Zhong et al., 2015).

525   Considering the chemically reactive species, NO concentrations are slightly underestimated on both
526   sides of the canyon as for the regular canyon, with the maximum difference of 74.9 ppb (9.5%) in
527    $Box_{[1,4]}$ on the windward corner. NO_2 is overestimated by the 32-box model, especially for the
528   windward side (~6%). The O_3 concentrations are slightly underestimated by the 32-box model in the
529   upper vortex on the windward side (~5%), and then are overestimated when air parcel moves to the
530   upper leeward side and to the lower vortex (~10%). Although HO_x concentrations are still higher in
531   the 32-box model compared to the LES, the spatial profiles of HO_2 are well reproduced due to a longer
532   diffusion time in the deep canyon in contrast to the regular canyon. Errors in modelled concentrations
533   (solid and dash lines with the same color) always become larger at $0 < z/l_0 < 1.0$ but become closer at
534    $1.0 < z/l_0 < 2.0$. For example, the 32-box model overestimates NO_2 and O_3 by 14.9% and 27.4% on
535   the leeward side, and by 18.1% and 23.1% on the windward side at the street level ($0 < z/l_0 < 0.25$),
536   but those differences decrease to 8.1%, 17.8%, 14.4% and -10.0% at the rooftop level ($0.75 < z/l_0 <$
537   1.0), respectively. Therefore, when applying the grid assumption to simulate reactive species in street
538   canyons, it is necessary to consider the inherent uncertainty due to chemical reactions being too fast
539   in particular at the street level, which may lead to an overestimation of pedestrian exposure risks.

540   3.3. The model performance with the simple NO_x-O_3 cycle

541   The performance of the multi-box models has been further evaluated with the simplified NO_x-O_3
542   chemical reactions:

543    $$NO + O_3 \rightarrow NO_2 \qquad\qquad\qquad (23)$$

544    $$NO_2 + hv \xrightarrow{O_2} NO + O_3 \qquad\qquad\qquad (24)$$

545   where hv represents solar photons. The production and photodegradation coefficients of NO_2 are
546   taken from the RCS chemistry, which are 4.01×10^{-4} ppb^{-1} s^{-1} and 9.20×10^{-3} s^{-1}, respectively. The
547   QSSA is adopted for the calculation. The computation time for the multi-box model using the simple
548   NO_x-O_3 cycle is much quicker (~40 s) than that using RCS chemistry. Table 4 illustrates the time-
549   and spatial-averaged mixing-ratios of NO, NO_2, O_3, NO_x, O_x and NO_2/NO ratios with solely NO_x-O_3
550   reactions during the final hour in the regular and deep canyons. The modelled NO_x concentrations of
551   the LES model are about 1.9% lower in the regular canyon but are slightly higher in the deep canyon
552   compared to the box models, partly because of strong turbulent fluctuations in the LES. As expected,
553   NO_2 concentrations gradually reduce by 10-13% in the regular canyon without involving OH/HO_2
554   chemicals, thereby decreasing O_x contents to a similar magnitude. This reduction is rather significant
555   (37-41%) in the deep canyon, resulting in dramatically lower NO_2/NO ratios, which is demonstrated
556   by Zhong et al. (2017). In comparison with the LES outputs, O_3 concentrations are underestimated
557   by the box models to different extents in both regular and deep canyons, which differs from its trends
558   of overestimation with the RCS chemistry. Overall the multi-box models performed better than the
559   one-box and two-box models in simulating all reactive species except O_3.

560   Modelling differences between the four models shrink when using the very simplified chemical
561   reactions in contrast to the NO_x-O_3-VOC chemical scheme. More specifically, Fig. 5 presents vertical
562   profiles of the difference of NO, NO_2 and O_3 concentrations under different chemical schemes using
563   the multi-box models and the LES, respectively. It clearly exhibits the direct contributions from the
564   VOCs mechanisms spatially, which, in general, shows more substantial influences on the modelling
565   results of the multi-box model compared to those of the LES. The contributions of VOCs are
566   significantly enhanced in the deep street canyon compared to the regular canyon; involving VOCs

567   tends to have greater impacts on local emitted species such as NO and NO_2 in the lower compartments

568   (i.e., $0 < z/l_0 < 1.0$) and on remote species such as O_3 in the upper compartments (i.e., $1.0 < z/l_0 < 2.0$).

569   Although there are some differences between the performance of the multi-box models and the LES,

570   the multi-box models reproduce well the contribution of VOCs to the vertical distribution of NO_2 and

571   O_3.

572   Fig. 6 illustrates the vertical distributions of NO, NO_2, and O_3 in the regular (a, b, c) and deep (d, e,

573   f) street canyons (i.e., horizontal-averaged concentration cross $-0.5 < x/l_0 < 0.5$) and along the canyon

574   walls (i.e., $-0.5 < x/l_0 < -0.25$ and $0.25 < x/l_0 < 0.5$). In the regular canyon, NO is well-simulated with

575   negligible difference between two models. The vertical profile of NO_2 is overestimated by the 16-box

576   model due to segregation. Nevertheless, extent of overestimation in NO_2 becomes smaller compared

577   to the simulations with NO_x-O_3-VOC chemistry, leading to relatively lower O_3 concentrations along

578   the leeward wall. However, underestimation of O_3 becomes larger on the windward side, with a

579   maximum difference of 4.8 ppb at the rooftop ($0.75 < z/l_0 < 1.0$). In the deep canyon, we also obtained

580   satisfied vertical distributions of all three species from the 32-box model compared to those in the

581   LES. Concentration gradients of NO_2 and O_3 lessen when applying the simple NO_x-O_3 cycle,

582   especially for the street level. NO_2 is still overestimated on the windward side and underestimated on

583   the leeward side, but to a much acceptable degree compared to the scenario with the RCS (Fig. 4).

584   The trends of O_3 are the same as that of the regular canyon in the upper vortex ($1.0 < z/l_0 < 2.0$), e.g.,

585   an underestimation on the windward side and overestimation on the leeward side but are consistent

586   with the LES in the lower vortex ($0 < z/l_0 < 1.0$). This indicates that the modelling domain with VOC

587   emissions (e.g., high coverage of vegetation) should consider using air quality models with resolution

588   as high possible to diminish the segregation effects in chemistry.

4. Conclusions

589

590   A process-based multi-box photochemical street-canyon model, with a flexible number of boxes and

591   based on a set of transport parameters calculated from the LES outputs is developed in this study. The

592   performance of this street-scale chemical transport model coupled with NO_x-O_3-VOC chemistry (or

593   a simplified NO_x-O_3 cycle), for modelling reactive species in the regular (AR = 1) and deep (AR = 2)

594   street canyons, is compared to published LES data and to one- and two-box simulations. Results show

595   that the model configured with a single box captures the average state of air pollutants in street

596 canyons, and the results are consistent with previous studies (Bright et al., 2013; Zhong et al., 2016).
597 Compared with the benchmark LES simulation, the multi-box model reproduces well the spatial
598 contrast in pollutant concentrations inside the street canyons in particular with a chemically inert
599 passive scalar. Namely, the spatial concentration patterns have been captured for the regular street
600 canyon (i.e., single primary vortex), as well as for the deep street canyon (i.e., two counter-rotating
601 vortices). For the regular canyon, it is found that the NO and O_3 titration reaction becomes more
602 effective due to less segregation along the windward facet, leading to an underestimate of O_3 and an
603 overestimate of NO_2 levels. On the leeward side, the overestimated NO_2 results in an overestimation
604 of O_3 through photolysis. An additional overestimation of NO_2 is attributed to OH/HO_2 chemistry.
605 The impact of segregation effects on the reactive species is substantial, in particular for short-lived
606 species. The OH and HO_2 concentrations are overestimated by the multi-box model, their vertical
607 variations are not very significant compared to the LES because of their very short chemical
608 timescales.
609 In a deep canyon with poor ventilation, the relationship of reactive species in the upper compartment
610 between the 32-box and LES models is consistent with those in the regular canyon. However, in the
611 lower compartments of the canyon, O_3 is always overestimated, and there are obvious variations of
612 OH and HO_2 concentrations along the vertical direction. Additionally, under the simple NO_x-O_3 cycle,
613 the differences between the multi-box model and the LES become smaller particularly for the deep
614 canyon. Although the effects of VOC chemistry on reactive species such as NO_2 are underestimated
615 compared to the LES, the multi-box models capture the vertical contribution of VOCs to these
616 pollutants in street canyons, and are a significant step forward from the simple one- and two-box
617 models. The multi-box model is less computationally efficient than the typical one-box (~1 s) and
618 two-box models (~8 s), but it can offer spatial information on reactive species within street canyons
619 based on coupled chemical-transport processes (with VOC chemistry) in a fairly short computational
620 times (~6 min) compared to the LES (e.g., ~10 days in Zhong et al. (2017)). Overall, the multi-box
621 model enables insightful investigations into the multiple processes as well as their complex
622 interactions and is of practical utility for air quality assessment or pollution mitigation management
623 in street canyons.
624 Further works may focus on adopting the multi-box model to simulate air pollution in street canyons
625 with spatially segregated emissions due to the presence of vegetation. More detailed chemical
626 schemes (e.g., Master Chemical Mechanism, MCM*v*3.0 (Saunders et al., 2003)) can be incorporated

627 into the model. The evaluation of modelling results with field measurements is recommended. A more

628 challenging task is to merge the effects of airflow parallel to the street axis on the diffusion and

629 transformation of chemical species, which would enable for a wider range of model applications.

636 **References**

637 Abhijith, K., Kumar, P., Gallagher, J., McNabola, A., Baldauf, R., Pilla, F., Broderick, B., Di Sabatino, S.,
638 Pulvirenti, B., 2017. Air pollution abatement performances of green infrastructure in open road and built-up
639 street canyon environments–A review. Atmospheric Environment 162 71-86.
640 Ahmad, K., Khare, M., Chaudhry, K., 2005. Wind tunnel simulation studies on dispersion at urban street
641 canyons and intersections—a review. Journal of Wind Engineering and Industrial Aerodynamics 93(9) 697-
642 717.
643 Alexandrov, V., Sameh, A., Siddique, Y., Zlatev, Z., 1997. Numerical integration of chemical ODE problems
644 arising in air pollution models. Environmental Modeling & Assessment 2(4) 365-377.
645 Baik, J.-J., Kang, Y.-S., Kim, J.-J., 2007. Modeling reactive pollutant dispersion in an urban street canyon.
646 Atmospheric Environment 41(5) 934-949.
647 Baker, J., Walker, H.L., Cai, X., 2004. A study of the dispersion and transport of reactive pollutants in and
648 above street canyons—a large eddy simulation. Atmospheric Environment 38(39) 6883-6892.
649 Boulter, P., Barlow, T., Latham, S., McCrae, I., 2009. Emission factors 2009: Report 1-a review of methods
650 for determining hotexhaust emission factors for road vehicles. TRL Published Project Report.
651 Bright, V.B., Bloss, W.J., Cai, X., 2013. Urban street canyons: Coupling dynamics, chemistry and within-
652 canyon chemical processing of emissions. Atmospheric Environment 68 127-142.
653 Cai, X.-M., Barlow, J., Belcher, S., 2008. Dispersion and transfer of passive scalars in and above street
654 canyons—large-eddy simulations. Atmospheric Environment 42(23) 5885-5895.
655 Cai, X., 2012. Effects of differential wall heating in street canyons on dispersion and ventilation
656 characteristics of a passive scalar. Atmospheric Environment 51 268-277.
657 Chew, L.W., Aliabadi, A.A., Norford, L.K., 2018. Flows across high aspect ratio street canyons: Reynolds
658 number independence revisited. Environmental Fluid Mechanics 18(5) 1275-1291.
659 Cui, Z., Cai, X., J. Baker, C., 2004. Large‐eddy simulation of turbulent flow in a street canyon. Quarterly
660 Journal of the Royal Meteorological Society 130(599) 1373-1394.
661 Driscoll, J.F., Chen, R.-H., Yoon, Y., 1992. Nitric oxide levels of turbulent jet diffusion flames: effects of
662 residence time and Damkohler number. Combustion and Flame 88(1) 37-49.
663 Eliasson, I., Offerle, B., Grimmond, C., Lindqvist, S., 2006. Wind fields and turbulence statistics in an urban

street canyon. Atmospheric Environment 40(1) 1-16.

Fellini, S., Ridolfi, L., Salizzoni, P., 2020. Street canyon ventilation: Combined effect of cross‑section geometry and wall heating. Quarterly Journal of the Royal Meteorological Society 146(730) 2347-2367.

Garmory, A., Kim, I., Britter, R., Mastorakos, E., 2009. Simulations of the dispersion of reactive pollutants in a street canyon, considering different chemical mechanisms and micromixing. Atmospheric Environment 43(31) 4670-4680.

Garmory, A., Richardson, E., Mastorakos, E., 2006. Micromixing effects in a reacting plume by the stochastic fields method. Atmospheric Environment 40(6) 1078-1091.

Gelbard, F., Seinfeld, J.H., 1980. Simulation of multicomponent aerosol dynamics. Journal of colloid and Interface Science 78(2) 485-501.

Gromke, C., Buccolieri, R., Di Sabatino, S., Ruck, B., 2008. Dispersion study in a street canyon with tree planting by means of wind tunnel and numerical investigations–evaluation of CFD data with experimental data. Atmospheric Environment 42(37) 8640-8650.

Gromke, C., Ruck, B., 2007. Influence of trees on the dispersion of pollutants in an urban street canyon— experimental investigation of the flow and concentration field. Atmospheric Environment 41(16) 3287-3302.

Heard, D.E., Pilling, M.J., 2003. Measurement of OH and HO_2 in the troposphere. Chemical Reviews 103(12) 5163-5198.

Jacobson, M.Z., Jacobson, M.Z., 2005. Fundamentals of atmospheric modeling. Cambridge university press.

Jacobson, M.Z., Seinfeld, J.H., 2004. Evolution of nanoparticle size and mixing state near the point of emission. Atmospheric Environment 38(13) 1839-1850.

Jacobson, M.Z., Tabazadeh, A., Turco, R.P., 1996. Simulating equilibrium within aerosols and nonequilibrium between gases and aerosols. Journal of Geophysical Research: Atmospheres 101(D4) 9079-9091.

Jasak, H., Jemcov, A., Tukovic, Z., 2007. OpenFOAM: A C++ library for complex physics simulations, International workshop on coupled methods in numerical dynamics. IUC Dubrovnik Croatia, pp. 1-20.

Kim, M.J., Park, R.J., Kim, J.-J., 2012. Urban air quality modeling with full O3–NOx–VOC chemistry: Implications for O3 and PM air quality in a street canyon. Atmospheric Environment 47 330-340.

Kovar-Panskus, A., Louka, P., Sini, J.-F., Savory, E., Czech, M., Abdelqari, A., Mestayer, P., Toy, N., 2002. Influence of geometry on the mean flow within urban street canyons–a comparison of wind tunnel experiments and numerical simulations. Water, air and soil pollution: focus 2(5) 365-380.

Krol, M.C., Molemaker, M.J., de Arellano, J.V.G., 2000. Effects of turbulence and heterogeneous emissions on photochemically active species in the convective boundary layer. Journal of Geophysical Research: Atmospheres 105(D5) 6871-6884.

Kukkonen, J., Olsson, T., Schultz, D., Baklanov, A., Klein, T., Miranda, A., Monteiro, A., Hirtl, M., Tarvainen, V., Boy, M., 2012. A review of operational, regional-scale, chemical weather forecasting models in Europe. Atmospheric Chemistry and Physics 12(1) 1-87.

Kwak, K.-H., Baik, J.-J., 2012. A CFD modeling study of the impacts of NOx and VOC emissions on reactive pollutant dispersion in and above a street canyon. Atmospheric Environment 46 71-80.

Lee, J.D., Lewis, A.C., Monks, P.S., Jacob, M., Hamilton, J.F., Hopkins, J.R., Watson, N.M., Saxton, J.E., Ennis, C., Carpenter, L.J., 2006. Ozone photochemistry and elevated isoprene during the UK heatwave of August 2003. Atmospheric Environment 40(39) 7598-7613.

Li, X.-X., Leung, D.Y., Liu, C.-H., Lam, K.M., 2008. Physical modeling of flow field inside urban street canyons. Journal of Applied Meteorology and Climatology 47(7) 2058-2067.

Lietzke, B., Vogt, R., 2013. Variability of CO_2 concentrations and fluxes in and above an urban street canyon. Atmospheric Environment 74 60-72.

Liu, C.-H., Leung, D.Y., 2008. Numerical study on the ozone formation inside street canyons using a chemistry box model. Journal of Environmental Sciences 20(7) 832-837.

Murena, F., 2012. Monitoring and modelling carbon monoxide concentrations in a deep street canyon: application of a two-box model. Atmospheric pollution research 3(3) 311-316.

713   Murena, F., Favale, G., Vardoulakis, S., Solazzo, E., 2009. Modelling dispersion of traffic pollution in a deep
714   street canyon: Application of CFD and operational models. Atmospheric Environment 43(14) 2303-2311.
715   Nikolova, I., MacKenzie, A.R., Cai, X., Alam, M.S., Harrison, R.M., 2016. Modelling component evaporation
716   and composition change of traffic-induced ultrafine particles during travel from street canyon to urban
717   background. Faraday discussions 189 529-546.
718   Oke, T.R., 1988. Street design and urban canopy layer climate. Energy and buildings 11(1-3) 103-113.
719   R Core Team, T., 2019. R: A language and environment for statistical computing. Vienna, Austria.
720   Salizzoni, P., Soulhac, L., Mejean, P., 2009. Street canyon ventilation and atmospheric turbulence.
721   Atmospheric Environment 43(32) 5056-5067.
722   Saunders, S.M., Jenkin, M.E., Derwent, R., Pilling, M., 2003. Protocol for the development of the Master
723   Chemical Mechanism, MCM v3 (Part A): tropospheric degradation of non-aromatic volatile organic
724   compounds. Atmospheric Chemistry and Physics 3(1) 161-180.
725   Schlichting, H., Gersten, K., 2016. Boundary-layer theory. Springer.
726   Takano, Y., Moonen, P., 2013. On the influence of roof shape on flow and dispersion in an urban street
727   canyon. Journal of Wind Engineering and Industrial Aerodynamics 123 107-120.
728   Vardoulakis, S., Fisher, B.E., Pericleous, K., Gonzalez-Flesca, N., 2003. Modelling air quality in street
729   canyons: a review. Atmospheric Environment 37(2) 155-182.
730   Watson, L., Shallcross, D., Utembe, S., Jenkin, M., 2008. A Common Representative Intermediates (CRI)
731   mechanism for VOC degradation. Part 2: Gas phase mechanism reduction. Atmospheric Environment 42(31)
732   7196-7204.
733   Wu, L., Hang, J., Wang, X., Shao, M., Gong, C., 2021. APFoam 1.0: integrated computational fluid dynamics
734   simulation of O 3–NO x–volatile organic compound chemistry and pollutant dispersion in a typical street
735   canyon. Geoscientific Model Development 14(7) 4655-4681.
736   Yang, H., Chen, T., Lin, Y., Buccolieri, R., Mattsson, M., Zhang, M., Hang, J., Wang, Q., 2020. Integrated
737   impacts of tree planting and street aspect ratios on CO dispersion and personal exposure in full-scale street
738   canyons. Building and Environment 169 106529.
739   Yang, H., Lam, C.K.C., Lin, Y., Chen, L., Mattsson, M., Sandberg, M., Hayati, A., Claesson, L., Hang, J.,
740   2021. Numerical investigations of Re-independence and influence of wall heating on flow characteristics and
741   ventilation in full-scale 2D street canyons. Building and Environment 189 107510.
742   Zhang, K., Chen, G., Zhang, Y., Liu, S., Wang, X., Wang, B., Hang, J., 2020. Integrated impacts of turbulent
743   mixing and NOX-O3 photochemistry on reactive pollutant dispersion and intake fraction in shallow and deep
744   street canyons. Science of the Total Environment 712 135553.
745   Zhong, J., Cai, X.-M., Bloss, W.J., 2015. Modelling the dispersion and transport of reactive pollutants in a
746   deep urban street canyon: Using large-eddy simulation. Environmental Pollution 200 42-52.
747   Zhong, J., Cai, X.-M., Bloss, W.J., 2016. Modelling photochemical pollutants in a deep urban street canyon:
748   application of a coupled two-box model approximation. Atmospheric Environment 143 86-107.
749   Zhong, J., Cai, X.-M., Bloss, W.J., 2017. Large eddy simulation of reactive pollutants in a deep urban street
750   canyon: Coupling dynamics with O_3-NO_x-VOC chemistry. Environmental Pollution 224 171-184.
751   Zhong, J., Nikolova, I., Cai, X., MacKenzie, A.R., Alam, M.S., Xu, R., Singh, A., Harrison, R.M., 2020a.
752   Neighbourhood-scale dispersion of traffic-induced ultrafine particles in central London: WRF large eddy
753   simulations. Environmental Pollution 266 115223.
754   Zhong, J., Nikolova, I., Cai, X., MacKenzie, A.R., Alam, M.S., Xu, R., Singh, A., Harrison, R.M., 2020b.
755   Traffic-induced multicomponent ultrafine particle microphysics in the WRF v3. 6.1 large eddy simulation
756   model: General behaviour from idealised scenarios at the neighbourhood-scale. Atmospheric Environment
757   223 117213.
758   Zhong, J., Nikolova, I., Cai, X., MacKenzie, A.R., Harrison, R.M., 2018. Modelling traffic-induced
759   multicomponent ultrafine particles in urban street canyon compartments: Factors that inhibit mixing.
760   Environmental Pollution 238 186-195.
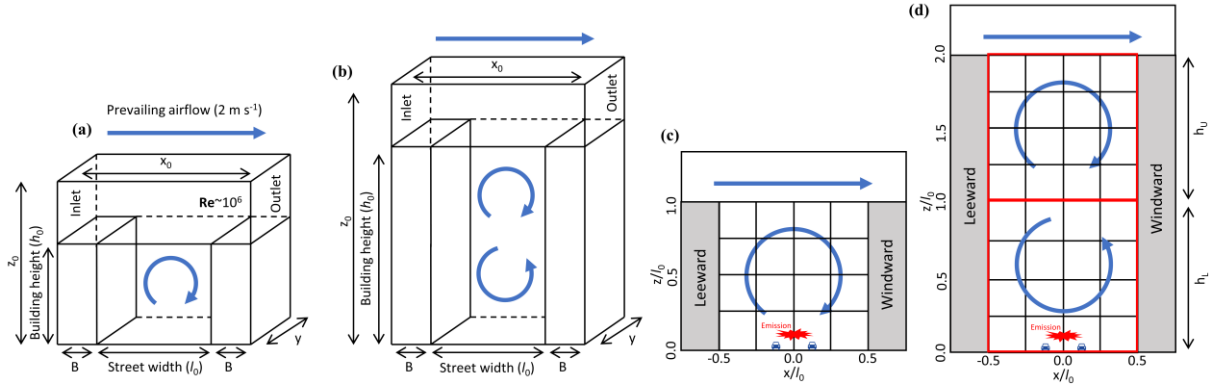761

Figures

Fig. 1. Schematic diagram of (a) the LES domain for a regular urban street canyon where $x_0 = 24$ m, $y_0 = 40$ m and $z_0 = 90$ m, and canyon geometries $l_0 = h_0 = 18$ m, wall width B = 3 m, modified from Bright et al. (2013); (b) the LES domain for a deep canyon $x_0 = 36$ m, $y_0 = 40$ m and $z_0 = 112$ m, and canyon geometries $l_0 = 18$ m, $h_0 = 36$ m and B = 9 m, modified from Zhong et al. (2015); (c) the equivalent multi-box (16) model for the regular canyon; (d) the two-box model denoted by the red frame, where the height of upper (h_U) and lower compartments (h_L) is 9 m, and the multi-box (32) model for the deep canyon. See text for details.
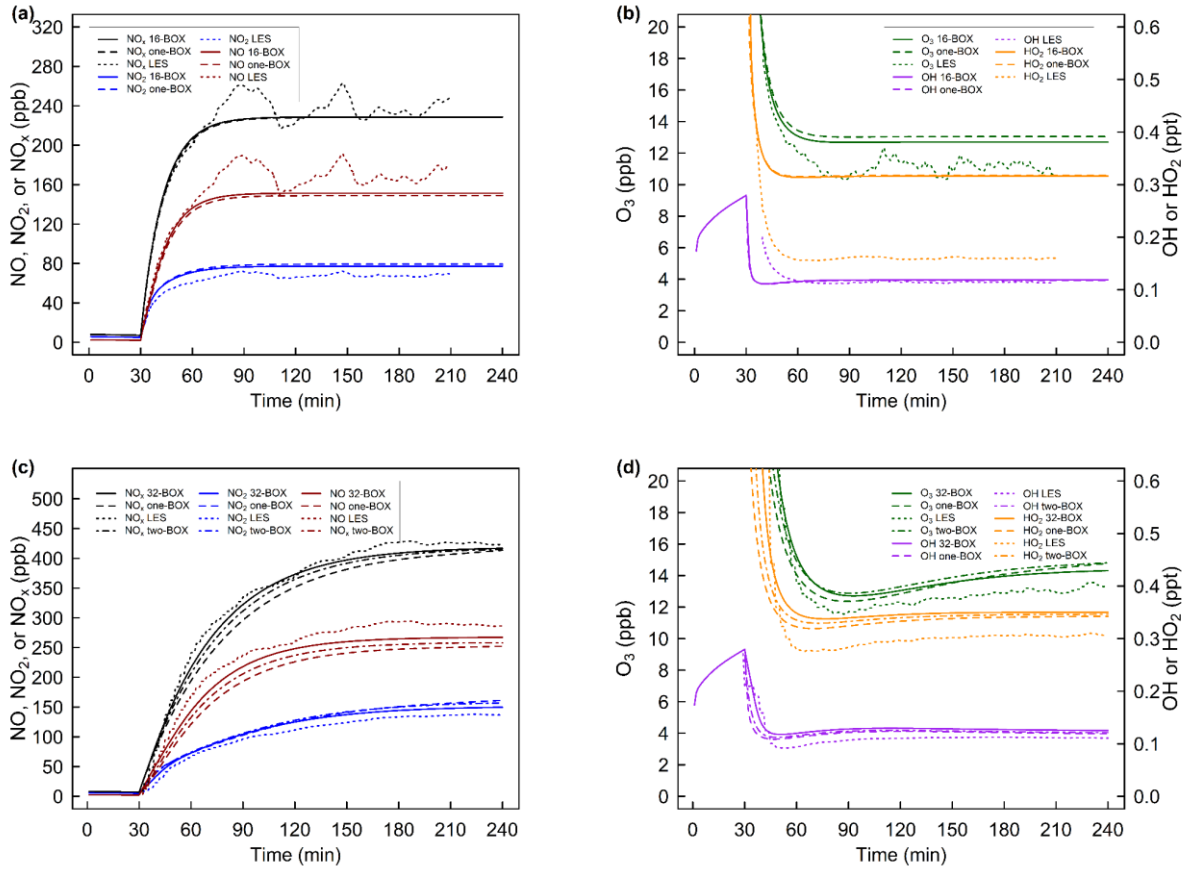
Fig. 2. Temporal variation of the spatially averaged mixing-ratio of NO, NO$_2$, NO$_x$, O$_3$ (ppb), OH and HO$_2$ (ppt) calculated using the LES, multi-box and a typical one-box models for the regular (a, b) and deep (c, d) street canyons. Two-box simulations are conducted only in the deep canyon, see text for details.
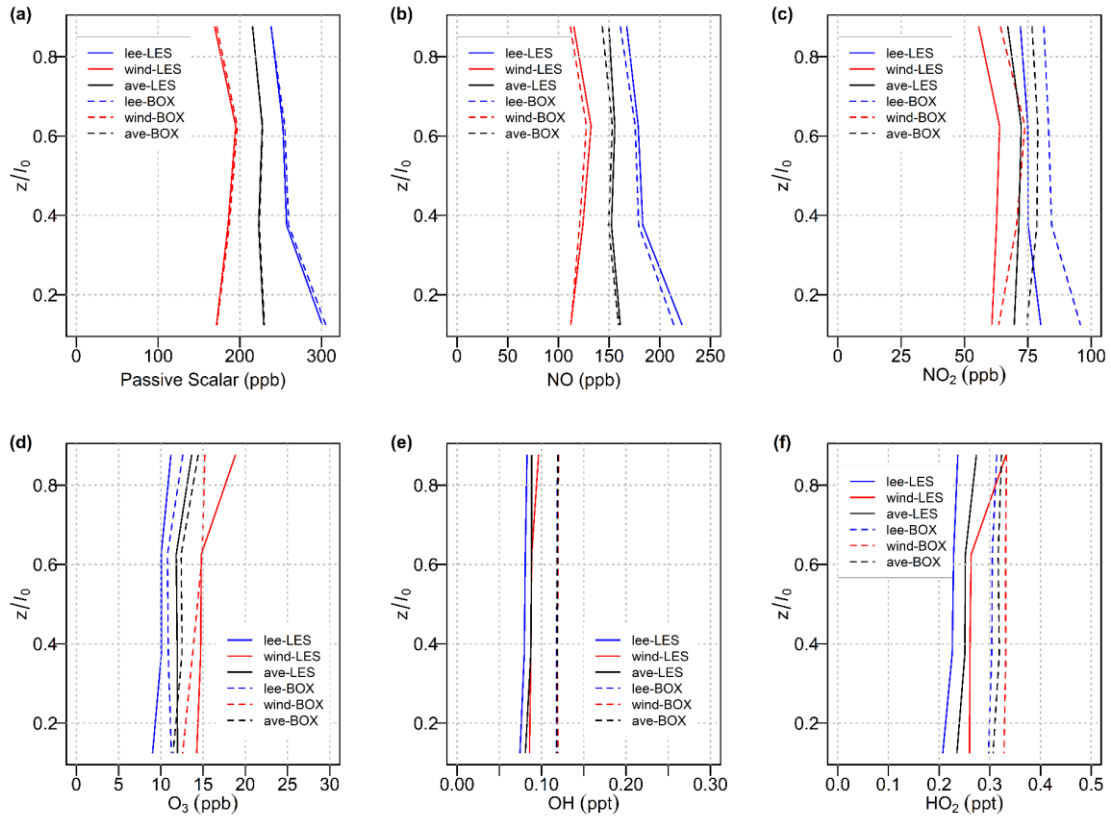
Fig. 3. Vertical profiles of the time-averaged mixing-ratios of PS, NO, NO$_2$, O$_3$, OH and HO$_2$ in the regular street canyon ($-0.5 < x/l_0 < 0.5$) represented by the black lines, along with the leeward wall ($-0.5 < x/l_0 < -0.25$) represented the by blue lines, and along with the windward wall ($0.25 < x/l_0 < 0.5$) represented by the red lines. Solid and dash lines indicate modelling results from LES and multi-box models, respectively.
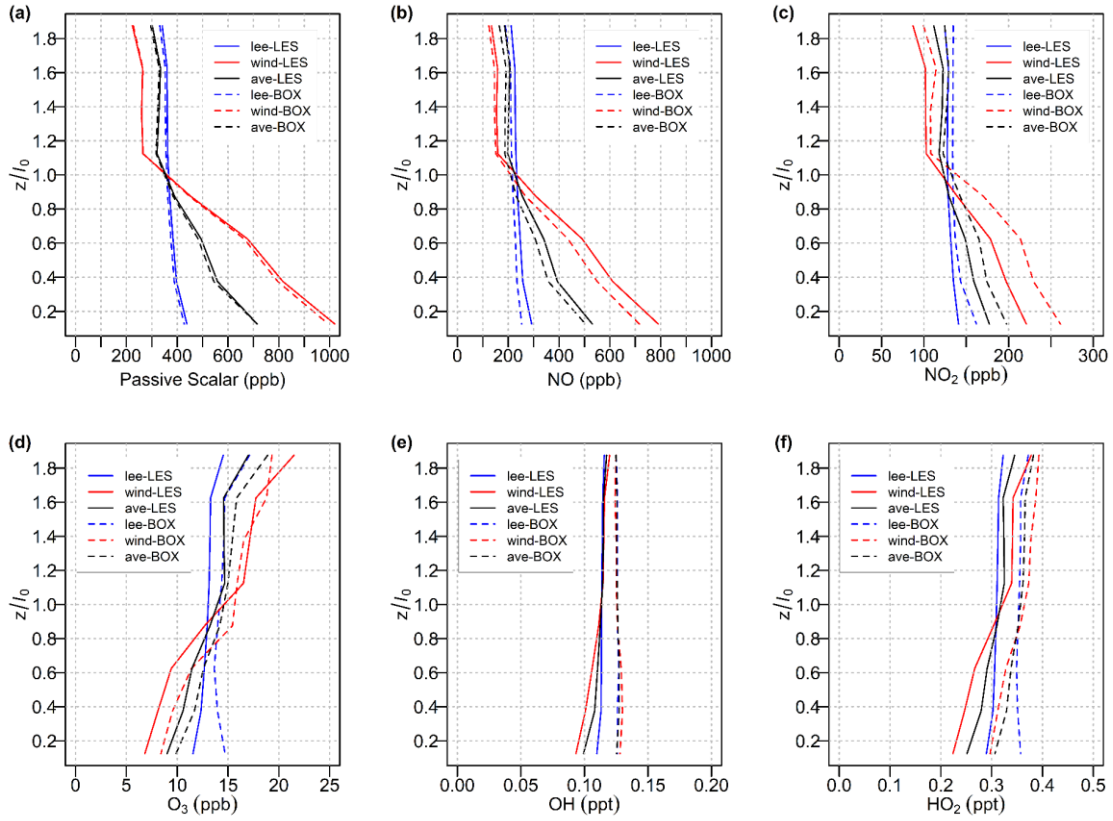
Fig. 4. Vertical profiles of the time-averaged mixing-ratios of PS, NO, NO$_2$, O$_3$, OH and HO$_2$ in the deep street canyon (-0.5 < x/l_0 < 0.5) represented by the black lines, along with the leeward wall (-0.5 < x/l_0 < -0.25) represented the by blue lines, and along with the windward wall (0.25 < x/l_0 < 0.5) represented by the red lines. Solid and dash lines indicate modelling results from LES and multi-box models, respectively.
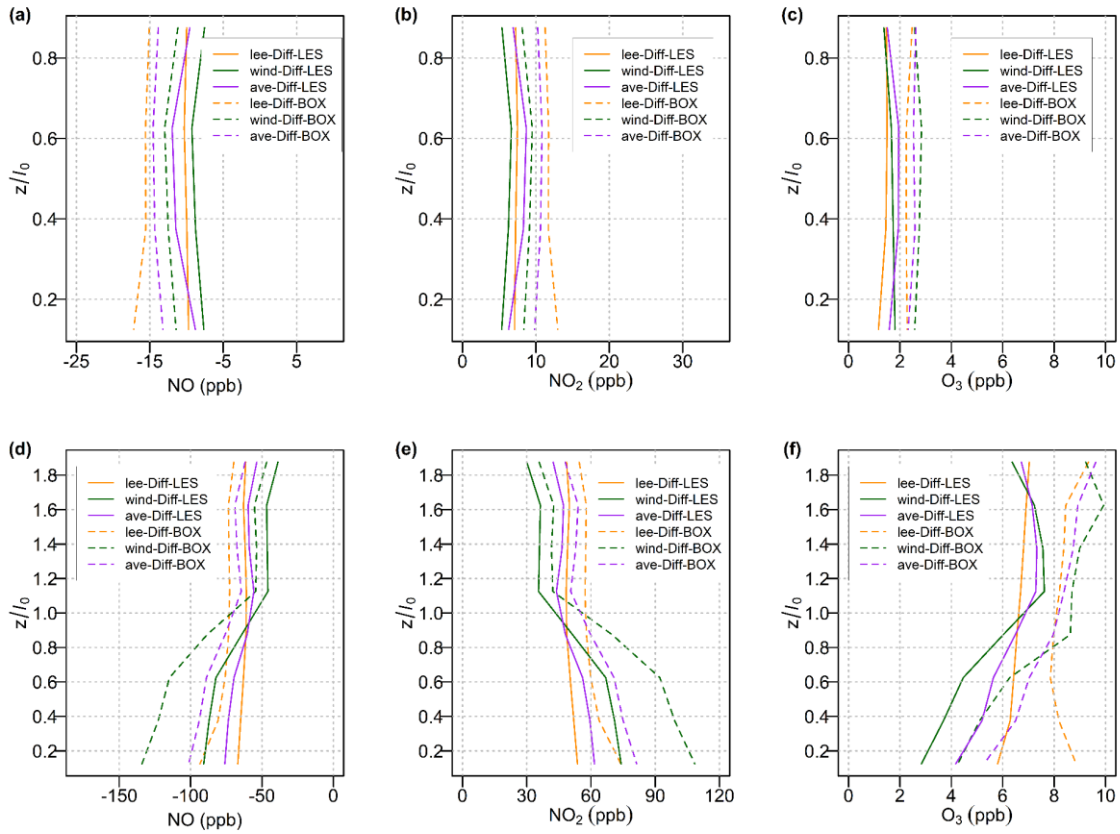
Fig. 5. Vertical profiles of the difference of NO, NO_2 and O_3 concentrations under different chemical schemes (modelling results with the VOC chemistry minus results with the simple NO_x-O_3 chemistry) in regular (a, b, c) and deep (d, e, f) street canyons (-0.5 < x/l_0 < 0.5) represented by the purple lines, along with the leeward wall (-0.5 < x/l_0 < -0.25) represented the by orange lines, and along with the windward wall (0.25 < x/l_0 < 0.5) represented by the green lines. Solid and dash lines indicate modelling results from LES and multi-box models, respectively.

Fig. 6. Vertical profiles of the time-averaged mixing-ratios of NO, NO_2, and O_3 in regular (a, b, c) and deep (d, e, f) street canyons (-0.5 < x/l_0 < 0.5) represented by the black lines, along with the leeward wall (-0.5 < x/l_0 < -0.25) represented the by blue lines, and along with the windward wall (0.25 < x/l_0 < 0.5) represented by the red lines. Solid and dash lines indicate modelling results from LES and multi-box models, respectively.
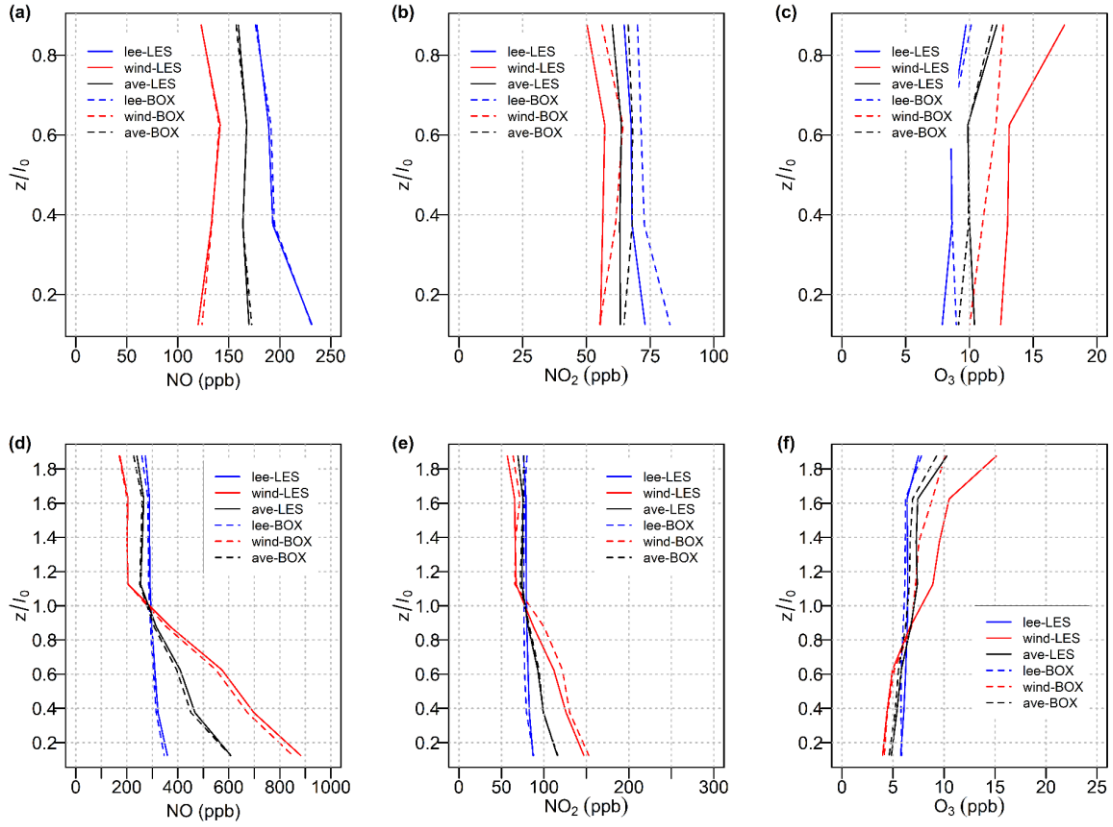
Tables

Table 1. Time-averaged mixing-ratios from LES, the multi (16/32)-box model, and the one-box and two-box models with RCS chemistry for urban street canyons.

		Mixing-ratio (ppb)				(b) - (a)	(c) - (a)	(d) - (a)	[(b)-(a)]/(a) (%)	[(c)-(a)]/(a) (%)	[(d)-(a)]/(a) (%)
		(a) LES	(b) 16/32-box	(c) Two-box	(d) One-box						
The regular street canyon (AR = 1)	PS	223.86	224.33	-	223.85	0.47	-	-0.01	0.21	-	-0.004
	NO	154.66	151.28	-	148.87	-3.38	-	-5.79	-2.19	-	-3.74
	NO_2	70.12	77.19	-	79.35	7.07	-	9.23	10.08	-	13.16
	O_3	12.35	12.70	-	13.05	0.35	-	0.70	2.83	-	5.67
	OH^*	0.086	0.119	-	0.118	0.033	-	0.032	38.37	-	37.21
	HO_2^*	0.253	0.316	-	0.318	0.063	-	0.065	24.90	-	25.69
	NO_x	224.78	228.47	-	228.22	3.69	-	3.44	1.64	-	1.51
	O_x	82.47	89.89	-	92.4	7.42	-	9.93	9.00	-	11.05
	NO_2/NO	0.45	0.51	-	0.53						
The deep street canyon (AR = 2)	PS	430.23	423.53	421.53	417.06	-6.7	-8.7	-13.17	-1.56	-2.02	-3.06
	NO	289.10	266.48	257.48	250.11	-22.62	-31.62	-38.99	-7.82	-10.94	-13.49
	NO_2	136.07	147.84	154.57	156.52	11.77	18.5	20.45	8.65	13.60	15.03
	O_3	13.14	14.19	14.62	14.46	1.05	1.48	1.32	7.99	11.26	10.05
	OH^*	0.11	0.13	0.12	0.12	0.02	0.01	0.01	18.18	9.09	9.09
	HO_2^*	0.31	0.35	0.34	0.34	0.04	0.03	0.03	12.90	9.68	9.68
	NO_x	425.17	414.32	412.05	406.63	-10.85	-13.12	-18.54	-2.55	-3.09	-4.47
	O_x	149.21	162.03	169.19	170.98	12.82	19.98	21.77	8.59	13.39	13.44
	NO_2/NO	0.47	0.55	0.60	0.63						

* Mixing-ratio of OH and HO_2 are presented in part per trillion (ppt).

Table 2. Time-averaged mixing-ratios from LES, the 32-box model and the two-box model with RCS chemistry in the deep canyon.

		Mixing-ratio (ppb)					[(b)-(a)]/(a) (%)	[(c)-(a)]/(a) (%)
		(a) LES	(b) 32-box	(c) Two-box	(b) - (a)	(c) - (a)		
The upper compartment	PS	321.23	315.93	313.65	-5.30	-7.58	-1.65	-2.36
	NO	198.14	182.87	178.03	-15.27	-20.11	-7.71	-10.15
	NO_2	118.44	125.78	129.02	7.34	10.58	6.20	8.93
	O_3	15.21	16.29	16.96	1.08	1.75	7.10	11.51
	OH^*	0.11	0.12	0.12	0.01	0.01	9.09	9.09
	HO_2^*	0.33	0.36	0.37	0.03	0.04	9.09	12.12
	NO_x	316.58	308.65	307.05	-7.93	-9.53	-2.50	-3.01
	O_x	133.65	142.06	145.97	8.41	12.32	6.29	9.22
	NO_2/NO	0.60	0.68	0.72				
The lower compartment	PS	539.23	531.13	529.42	-8.10	-9.81	-1.50	-1.82
	NO	380.06	350.09	336.93	-29.97	-43.13	-7.89	-11.35
	NO_2	153.69	169.90	180.12	16.21	26.43	10.55	17.20
	O_3	11.06	12.09	12.29	1.03	1.23	9.31	11.12
	OH^*	0.11	0.12	0.12	0.01	0.01	9.09	9.09
	HO_2^*	0.28	0.33	0.33	0.05	0.05	17.86	17.86
	NO_x	533.75	519.99	517.05	-13.76	-16.7	-2.58	-3.13
	O_x	164.75	181.99	192.41	17.24	27.66	10.46	16.79
	NO_2/NO	0.40	0.48	0.53				

* Mixing-ratio of OH and HO_2 are presented in part per trillion (ppt).

Table 3. The percentage intensities of segregation between pairs of reactive species from the LES and multi-box models (BOX) for the regular and deep canyons. Bold symbols represent species that directly react with each other in the models, and negative values are shown in red.

		LES					BOX				
		NO	NO_2	O_3	OH	HO_2	NO	NO_2	O_3	OH	HO_2
	NO	3.02	-	-	-	-	2.97	-	-	-	-
	NO_2	1.38	0.83	-	-	-	1.61	1.15	-	-	-
The regular street canyon (AR = 1)	O_3	**-2.79**	-1.64	3.54	-	-	**-1.34**	-0.36	1.61	-	-
	OH	**-0.81**	**-0.27**	**0.76**	0.43	-	**-0.08**	**-0.03**	**0.07**	0.004	-
	HO_2	**-1.43**	**-0.71**	**1.74**	**0.60**	**1.12**	**-0.56**	**-0.20**	**0.42**	**0.02**	**0.15**
	NO	26.15	-	-	-	-	26.35	-	-	-	-
	NO_2	10.21	4.18	-	-	-	11.50	5.58	-	-	-
The deep street canyon (AR = 2)	O_3	**-10.02**	-4.35	5.09	-	-	**-9.35**	-3.86	4.45	-	-
	OH	**-2.75**	**-1.06**	**1.09**	0.31	-	**0.22**	**0.15**	**-0.09**	0.01	-
	HO_2	**-5.13**	**-2.12**	**2.36**	**0.57**	**1.15**	**-3.54**	**-1.45**	**1.56**	**-0.03**	**0.57**

Table 4. Time-averaged mixing-ratios from LES, the multi (16/32)-box model, and the one-box and two-box models with the simple NO_x-O_3 chemistry for urban street canyons.

| | | Mixing-ratio (ppb) | | | | | | | [(b)-(a)]/(a) (%) | [(c)-(a)]/(a) (%) | [(d)-(a)]/(a) (%) |
		(a) LES	(b) 16/32-box	(c) Two-box	(d) One-box	(b) - (a)	(c) - (a)	(d) - (a)			
The regular street canyon (AR = 1)	NO	165.10	165.27	-	163.24	0.17	-	-1.86	0.10	-	-1.13
	NO_2	62.58	66.81	-	68.72	4.22	-	6.14	6.75	-	9.81
	O_3	10.60	10.19	-	10.43	-0.41	-	-0.17	-3.89	-	-1.60
	NO_x	227.69	232.08	-	231.97	4.39	-	4.28	1.93	-	1.88
	O_x	73.18	77.00	-	79.16	3.81	-	5.97	5.21	-	8.16
	NO_2/NO	0.38	0.40	-	0.42						
The deep street canyon (AR = 2)	NO	352.57	344.33	336.85	333.14	-8.24	-15.72	-19.43	-2.34	-4.46	-5.51
	NO_2	85.43	86.30	90.29	92.03	0.87	4.86	6.60	1.02	5.69	7.72
	O_3	6.89	6.38	6.62	6.45	-0.51	-0.27	-0.44	-7.35	-3.95	-6.43
	NO_x	438.00	430.63	427.14	425.17	-7.37	-10.86	-12.83	-1.68	-2.48	-2.93
	O_x	92.32	92.69	96.91	98.48	0.37	4.59	6.15	0.40	4.97	6.67
	NO_2/NO	0.24	0.25	0.27	0.28						